

Crystal Structure of the Outer Membrane Protein OpdK from *Pseudomonas aeruginosa*

Shyamasri Biswas,^{1,4,5} Mohammad M. Mohammad,^{2,4} Liviu Movileanu,^{2,3} and Bert van den Berg^{1,*}

¹Program in Molecular Medicine, University of Massachusetts Medical School, Worcester, MA 01605, USA

²Department of Physics, Syracuse University, 201 Physics Building

³Structural Biology, Biochemistry, and Biophysics Program

Syracuse University, 111 College Place, Syracuse, NY 13244, USA

⁴These authors contributed equally to this work

⁵Present address: Department of Structural Biochemistry, 128 Polk Hall, North Carolina State University, Raleigh, NC 27695, USA

*Correspondence: bert.vandenbergh@umassmed.edu

DOI 10.1016/j.str.2008.04.009

SUMMARY

In Gram-negative bacteria that do not have porins, most water-soluble and small molecules are taken up by substrate-specific channels belonging to the OprD family. We report here the X-ray crystal structure of OpdK, an OprD family member implicated in the uptake of vanillate and related small aromatic acids. The OpdK structure reveals a monomeric, 18-stranded β barrel with a kidney-shaped central pore. The OpdK pore constriction is relatively wide for a substrate-specific channel (~ 8 Å diameter), and it is lined by a positively charged patch of arginine residues on one side and an electronegative pocket on the opposite side—features likely to be important for substrate selection. Single-channel electrical recordings of OpdK show binding of vanillate to the channel, and they suggest that OpdK forms labile trimers in the outer membrane. Comparison of the OpdK structure with that of *Pseudomonas aeruginosa* OprD provides the first qualitative insights into the different substrate specificities of these closely related channels.

INTRODUCTION

The outer membrane (OM) of Gram-negative bacteria forms an efficient barrier against the permeation of hydrophilic and hydrophobic molecules. To obtain the necessary ions and nutrients required for growth and function of the cell, transport channels are present within the OM. The passage of small, hydrophilic molecules across the OM is mediated by three classes of transport proteins: (1) general porins, (2) substrate-specific channels, and (3) active transporters, to which the TonB-dependent receptors belong. The porins and substrate-specific channels together are responsible for the uptake of virtually all small, hydrophilic molecules in Gram-negative bacteria. Transport mediated by porins and substrate-specific channels does not require energy, and it is not known to involve conformational changes in the protein (Nikaido, 2003).

General, or nonspecific, porins such as *Escherichia coli* OmpF and OmpC are present in a large number of Gram-negative bac-

teria. Most of these porins form trimeric, water-filled holes within the OM. They do not bind their substrates with appreciable affinity, and they mediate the passive diffusion of small (<600 Da) molecules according to their concentration gradients. A wealth of structural, biochemical, and genetic information is known about this class of OM channels (Nikaido, 2003). For substrates that are present at low concentrations in the external environment, passive diffusion is no longer efficient. For such molecules, OM passage is mediated by substrate-specific transporters, such as the maltose-specific channel LamB (Ishii et al., 1981) and the nucleoside-specific channel Tsx (Maier et al., 1988). This class of proteins, which includes both monomeric and trimeric channels, contains binding sites for their substrates, allowing for efficient transport at low substrate concentrations by facilitated diffusion.

Many Gram-negative bacteria, such as pseudomonads and other soil-dwelling microorganisms, do not have general porins (Hancock and Brinkman, 2002). Such bacteria depend on substrate-specific transporters for the uptake of small, water-soluble compounds. The OprD family, named after the prototype OprD protein from *Pseudomonas aeruginosa*, is the largest family of substrate-specific transporters currently known. In *P. aeruginosa*, the OprD family has 19 members, reflecting the remarkable metabolic versatility of this organism (Hancock and Brinkman, 2002). OprD family members are thought to be responsible for the uptake of the majority of small molecules in pseudomonads (Hancock and Brinkman, 2002), underscoring the importance of this family for the functioning of many Gram-negative bacteria, including plant and human pathogens. Besides being present in pseudomonads and related bacteria, OprD family members are also found in more divergent bacteria that do have general porins, such as *E. coli* and *Yersinia pestis* (Tamber et al., 2006). The function of OprD family members in these bacteria is not yet known.

All current knowledge about OprD family members has been obtained from studies of *P. aeruginosa* proteins. Besides being metabolically versatile, this bacterium is a well-known, opportunistic human pathogen, responsible for 10% of all hospital-acquired infections within the United States (Hancock and Brinkman, 2002). A severe problem in the treatment of patients infected with *P. aeruginosa* is the high intrinsic antibiotic resistance of this bacterium. The resistance is caused in part by the poorly permeable OM due to the absence of classical porins such as OmpF and OmpC. Thus, knowledge about the

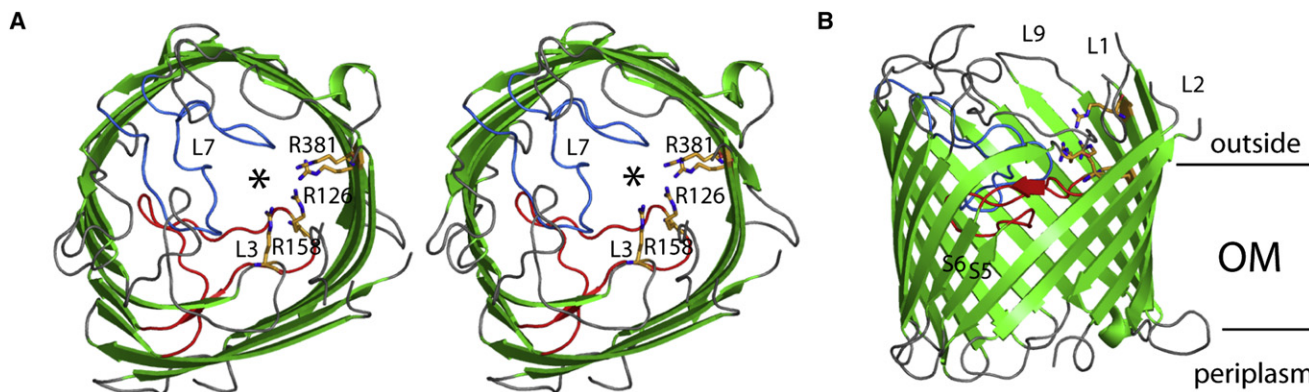


Figure 1. Overall Structure of OpdK

(A) Stereo cartoon of the OpdK backbone viewed from the extracellular side. β strands are green; loops are gray, with the exception of the pore-constricting loops L3 (red) and L7 (blue). The location of the OpdK pore is indicated with an asterisk. The residues of the arginine patch are shown as stick models with carbons colored orange, nitrogens colored blue, and oxygens colored red.

(B) Side view of OpdK, highlighting the short β strands S5 and S6. The approximate boundaries of the hydrophobic part of the outer membrane (OM) are indicated by horizontal lines. This and the following figures were made with PyMOL (DeLano, 2002).

structures and substrate transport mechanism of OprD family members could aid the design of drugs that can enter *P. aeruginosa* more efficiently.

The 19 OprD family members of *P. aeruginosa* are closely related, displaying ~45%–60% sequence similarity (30%–45% identity) (Hancock and Brinkman, 2002). Phylogenetic analysis showed that the family is comprised of two distinct groups (Tamber et al., 2006). The OprD subfamily comprises the smaller group, with eight members in *P. aeruginosa*. The other group, the OpdK subfamily, contains 11 members, most of which have not been characterized. The putative substrates of a number of OprD homologs have been identified by an indirect approach, involving the analysis of neighboring genes (genomic context) and transcription levels of *oprD* family genes in the presence of various substrates (Tamber et al., 2006). These analyses supported the previously proposed role of the archetypal OprD protein as a basic amino acid and carbapenem antibiotics channel (Trias and Nikaido, 1990), and identified vanillate (4-hydroxy-3-methoxy benzoate) and closely related aromatic acids as putative substrates for OpdK, the archetype of the OpdK subfamily (Tamber et al., 2006).

As a starting point to understand the structural basis and mechanism of substrate specificity and transport by OprD channels, we recently reported the X-ray crystal structure of OprD from *P. aeruginosa*, the first structure of any member of the OprD family of OM channels (Biswas et al., 2007). OprD forms an 18-stranded β barrel with a very narrow pore, formed by two inwardly folded extracellular loops. The location of conserved residues suggested that the OprD structure is representative of that of the entire OprD family. In order to confirm this prediction and to provide structural information on the OpdK subfamily of channels, we report here the X-ray crystal structure of OpdK from *P. aeruginosa* at 2.8 Å resolution. The basic architecture of the OpdK channel is indeed very similar to that of OprD; the OpdK pore, however, is shaped differently and is substantially larger than that of OprD, providing a structural rationale for the different substrate specificities of both channels. Single-channel electrical recording experiments with OpdK and vanil-

ate provide, to our knowledge, the first direct evidence for substrate binding to a member of the OprD family. Moreover, these experiments confirm the relatively large size of the OpdK pore and suggest that this channel forms labile trimers in the OM.

RESULTS AND DISCUSSION

Overall Structure of OpdK

P. aeruginosa OpdK was overexpressed in *E. coli* OMs and was purified by metal-affinity and size-exclusion chromatography (see Experimental Procedures). The structure of OpdK was solved by single-wavelength anomalous dispersion (SAD) with Se-Met-substituted protein. The final model of OpdK shows well-defined electron density for the entire molecule, with the exception of residues 70–80 in loop L2 and residues 25–32 in loop L1 (Figure 1). OpdK is present as a monomer in the crystals, with two molecules in the asymmetric unit. The structure shows an 18-stranded β barrel with long extracellular loops and short periplasmic turns. Interestingly, two of the β strands, S5 and S6, are too short to cover the entire hydrophobic part of the membrane (Figure 1).

The OpdK Pore Constriction

The OpdK pore constriction is kidney shaped, with the narrowest diameter being ~8 Å. The constriction is lined by residues from loops L3 (D123–R126), L4 (R158), L7 (S282–N294), and strand S18 (N379, R381). The distribution of charges around the pore is distinctly asymmetric (Figure 2), with positively charged amino acids on one side (R158, R126, R381, and R363), and (electro-)negatively charged residues on the other side (D123, D289, S282, and the backbone carbonyl of M290). The other residues that line the pore are G283, N292, N294, F291 (backbone carbonyl), and Q379 (Figure 2). In addition to the charge asymmetry at the pore constriction, a striking charge difference is also observed for the extracellular funnel and the periplasmic funnel. Whereas the extracellular funnel leading to the pore constriction is predominantly negatively charged (with the exception of the arginine patch; Figures 1A and 2A), the periplasmic funnel

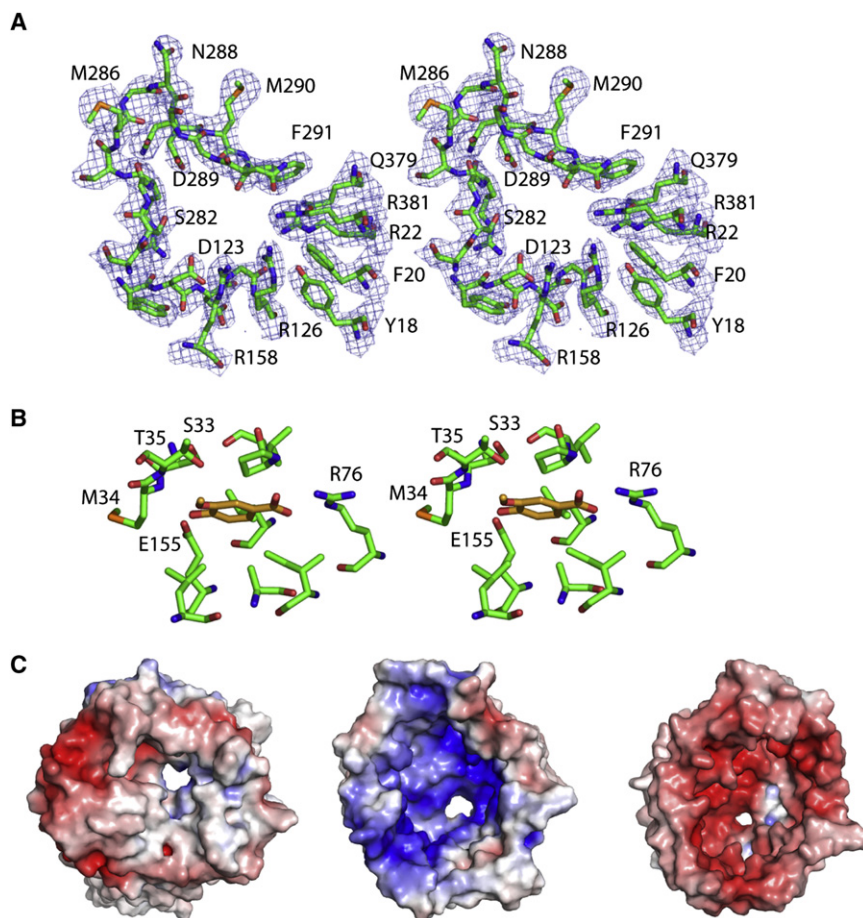


Figure 2. The OpdK Pore Constriction

(A) Stereoview from the extracellular side of the residues lining the OpdK pore, with $2F_o - F_c$ density shown as a blue mesh, contoured at 2.0σ . The orientation shown is similar to that in Figure 1A.

(B) Stereo cartoon view showing vanillate (colored orange, with oxygen atoms in red) bound to chorismate lyase (PDB code: 1XLR) (Smith et al., 2006). Carbons are green, oxygens are red, and nitrogens are blue.

(C) Electrostatic surface potential representation (made in PyMOL) of OpdK viewed from the extracellular side (left panel) and from the periplasmic side (middle panel). The surface is colored blue for potentials > 5 kT/e and red for potentials < -7 kT/e. The right panel shows the electrostatic surface of OprD viewed from the periplasmic side, colored blue for potentials > 10 kT/e and red for potentials < -10 kT/e.

leading from the constriction site is highly positively charged (Figure 2B).

Single-Channel Conductance Experiments

We performed single-channel electrical recordings with OpdK reconstituted in an artificial bilayer to investigate whether the relatively wide constriction of OpdK observed in the crystal structure is reflected by its capacity to conduct small ions. When we monitored the insertion of the channel at +40 mV, we observed a stepwise conductance of 345 ± 65 pS (13.8 ± 2.6 pA, $n = 3$) (Figure 3A), consistent with the presence of a relatively wide restriction in the structure. The single-channel electrical recordings showed a stable unitary conductance, but one decorated with transient current fluctuations, as shown by downward and upward spikes (Figure 3A, expanded part). It is likely that these current spikes are the result of movements of the extracellular loops within the pore lumen (Figure 3B). We also observed a reversed-mirror image of the current-voltage relationship in different single-channel experiments, suggesting that the OpdK protein inserts into the lipid bilayer in a bidirectional manner (Figure 3C).

Interestingly, although the crystal structure suggests that OpdK is a monomer, single-channel recordings under different conditions indicate that OpdK oligomerizes. We observed that OpdK also inserts into the lipid bilayer with higher conductance steps (Figure 4), depending on the protein concentration. When we added a greater amount of OpdK protein in the chamber

(8–10 ng/ μ l compared to 0.5–2 ng/ μ l, Figure 4A) and monitored the insertions at +40 mV, conductance values of 1250 ± 307 pS (50 ± 12 pA, $n = 5$) were obtained. This conductance is roughly three times that of the insertions at lower protein concentrations (Figure 4A). We observed both low- and high-conductance states in the same experiment at –20 mV (Figure 2B), again with the high-conductance values (1060 ± 200 pS; -21 ± 4 pA, $n = 3$) approximately three times that of the low-conductance values (300 ± 30 pS; -6 ± 0.6 pA, $n = 3$). These data suggest that OpdK oligomerizes in a concentration-dependent manner upon dilution from detergent solution, most likely forming trimers. In order to show closure of individual monomers within the trimer, we applied high voltages to the channels (+150 mV). This strategy was used previously for observing individual channel closures within the OmpF trimer (Basle et al., 2004). At these high voltages, we observed sharp closures with conductance values of 1366 ± 113 pS (205 ± 17 pA, $n = 3$) (Figure 4C), which does not correspond to closure of a single monomer at a time. However, we did observe transient current deflections (Figure 4C, expanded part) that are roughly equal to, double, or triple the individual single-channel conductance value of 380 ± 33 pS (57 ± 5 pA, $n = 3$). These deflections likely represent opening and closing of individual channels within the OpdK trimer.

Substrate Binding and Transport by OpdK

The putative assignment of vanillate and related compounds as substrates for the OpdK channel was derived indirectly from genetic context, transcriptional upregulation in the presence of substrates, and growth defects observed when an *opdk* deletion strain was grown with vanillate as the sole carbon source (Tamber et al., 2006). Inspection of the structure of chorismate lyase complexed with vanillate (Smith et al., 2006) does suggest that the pore constriction of OpdK could function as a binding site for vanillate. In chorismate lyase, the carboxyl group of vanillate

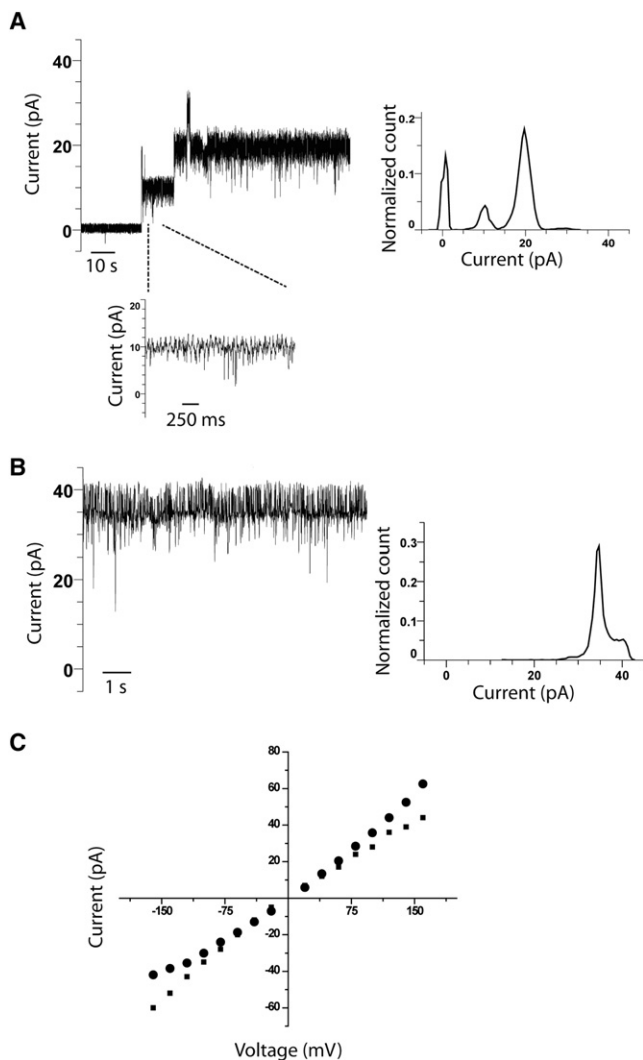


Figure 3. Single-Channel Electrical Recordings of the OpdK Protein

(A) Stepwise increase of the electrical current showing two single-channel insertions of the OpdK protein into the lipid bilayer. Protein (2 ng/ μ l) was added to the *cis* side of the lipid bilayer. The transmembrane potential was +40 mV. The expanded part of the trace shows the single-channel electrical trace at greater temporal resolution.

(B) The single-channel electrical signature at higher transmembrane potential (+100 mV). The right-hand panels show the most probable conductance states of the channel by using all-point amplitude Gaussian histograms.

(C) The OpdK protein inserts into the lipid bilayer bidirectionally. Shown are two current-voltage relationships for different single-channel recordings, suggesting bidirectional insertion of the OpdK protein (denoted by solid circles and solid squares for different directions of the insertion). Error bars were omitted for clarity. Single-channel electrical data were collected in 1 M KCl, 10 mM phosphate buffer (pH 7.4). The single-channel electrical signal was low-pass Bessel filtered at 0.1 kHz.

forms strong hydrogen bonds to the side chain of R76 (Figure 2B), as well as hydrogen bonds to a nearby water molecule and a backbone amide (L114). In OpdK, several closely spaced arginines could interact with the carboxyl group of the substrate, with Arg381 as the most likely candidate (Figures 1 and 2A). The 4-hydroxyl group of vanillate, located on the other

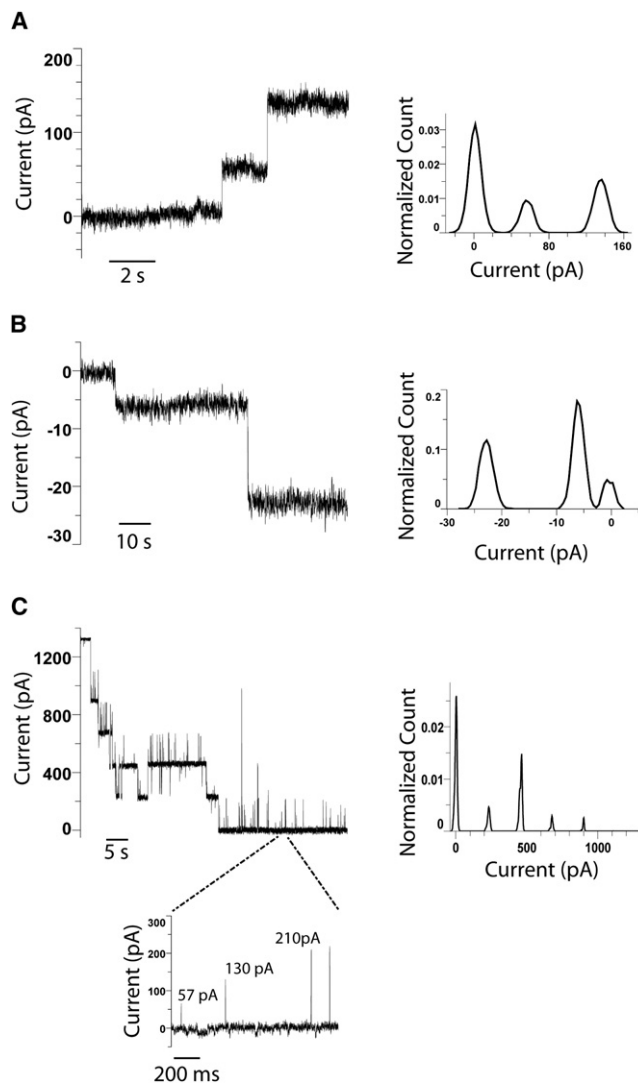


Figure 4. OpdK Forms Oligomers

(A) The electrical recording of successive high-conductance stepwise insertions. The conductances of first and second insertions are 1250 and 2000 pS, respectively. The insertions were observed at a transmembrane potential of +40 mV.

(B) Low- and high-conductance currents are observed within the same experiment. The conductance values of the first and second insertions are 300 and 880 pS, respectively. The insertions were monitored at -20 mV.

(C) The effect of higher voltage on the high-conductance OpdK states. Channels were formed at +40 mV until no further insertions occurred; subsequently, +150 mV was applied to monitor permanent closures of the pores. The expanded part of the trace shows the amplitude of the upward current deflections at greater temporal resolution. The conductance values of these current deflections, from left to right, are 380, 867, and 1400 pS, respectively. The right-hand panels show all-point amplitude Gaussian histograms to determine the most probable conductance values. The protein concentration was 8–10 ng/ μ l. Single-channel current recordings were carried out in 1 M KCl, 10 mM phosphate buffer (pH 7.4). Traces were filtered at 0.1 kHz.

side of the substrate, interacts in chorismate lyase with the carboxyl group of E155 and the backbone amide of M34 (Figure 2B). The 3-methoxy oxygen atom is also close to the M34 backbone amide, and it makes a hydrogen bond with the hydroxyl group of

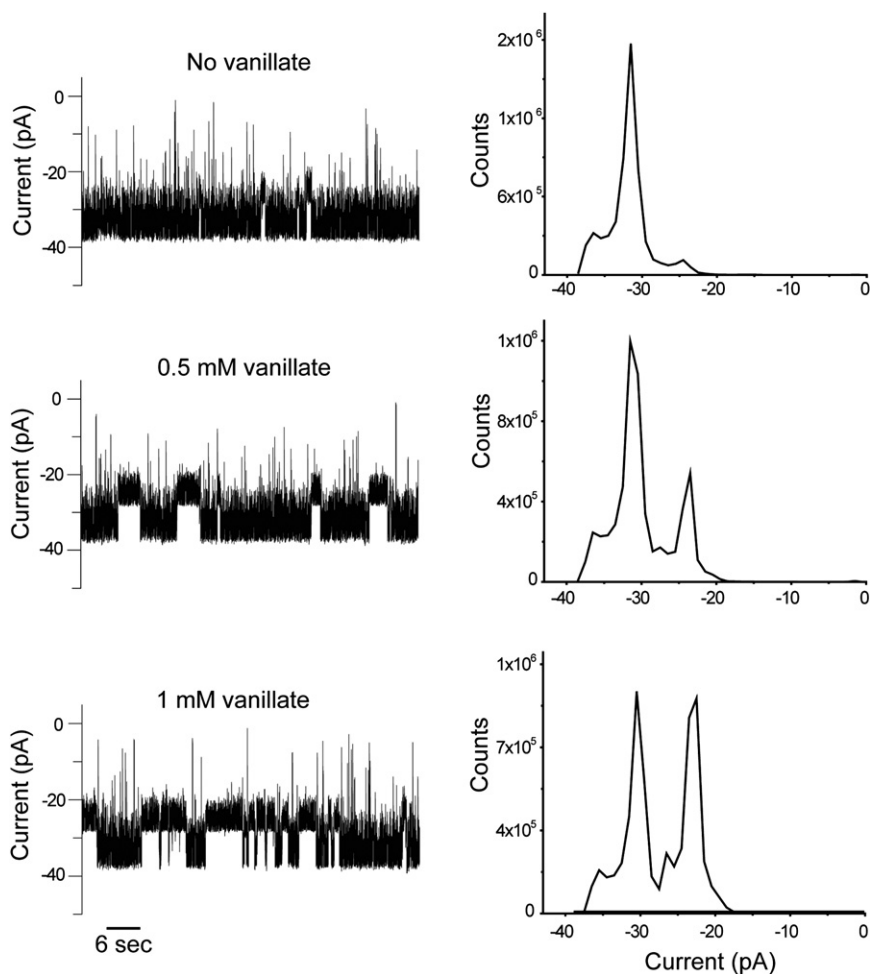


Figure 5. Binding of Vanillate to OpdK

A single OpdK pore was reconstituted in a planar lipid bilayer and tested for interaction with vanillate at 0.5 and 1 mM. The transmembrane potential was -80 mV. The right panels show all-point Gaussian amplitude histograms of the single-channel recordings before and after the addition of vanillate to the *cis* chamber. All single-channel electrical recordings were carried out in 1 M KCl, 10 mM potassium phosphate (pH 7.4). The single-channel electrical traces were low-pass Bessel filtered at 0.2 kHz.

T35. In OpdK, the S282 hydroxyl group, the backbone amide of G283, and the D289 carboxyl group (Figure 2A) are situated at the right side of the pore constriction to form hydrogen bonds with the vanillate hydroxyl and methoxy group. Furthermore, the closest distance between the R382 side chain on one side of the constriction and S282/D289 on the other side (Figure 2A) is large enough (~ 10 Å) to allow for insertion of a vanillate molecule. We propose that the larger size of the OpdK pore relative to OprD functions to accommodate the rigid shape and larger footprint of the vanillate substrate, requiring an elongated pore with hydrogen-bonding partners located on both sides. By contrast, the OprD substrate arginine is much more flexible and has a smaller footprint than vanillate, allowing for the presence of a very narrow pore in OprD. Thus, the architecture of the OpdK pore constriction is consistent with OpdK functioning as a vanillate channel.

Thus far, we have not been able to obtain well-diffracting cocrystals of OpdK and vanillate. This could be due to the relatively low solubility of vanillate in water (~ 50 mM; substantially less in many crystallization conditions), coupled to a possibly low affinity of OpdK for substrate under the crystallization conditions. We therefore attempted to observe substrate binding to OpdK at physiological pH by using single-channel conductance experiments. The blockage of ion current in single-channel conduc-

tance experiments has been used to probe substrate binding to a number of different substrate-specific OM channels under more physiological conditions (Bezrukov et al., 2000). Single-channel electrical recordings of OpdK in the presence of vanillate (added to the *cis* chamber) showed long-lived current blockades, with frequencies that were dependent on the substrate concentration (Figure 5). At concentrations of 0.5 and 1 mM vanillate, we measured event frequencies of 0.08 s $^{-1}$ and 0.2 s $^{-1}$, respectively ($n = 3$), indicating a proportionality between the substrate concentration and the frequency of substrate-induced blockage events. The rate constants of association (k_{on}) and dissociation (k_{off}) for the interaction of vanillate with the OpdK pore were $(2.1 \pm 0.2) \times 10^2$ M $^{-1}$ s $^{-1}$ and $(4.1 \pm 0.1) \times 10^{-1}$ s $^{-1}$ ($n = 3$), respectively

(Experimental Procedures), yielding a dissociation constant (KD) of 2 mM. To our knowledge, these single-channel data provide the first direct evidence for an interaction between substrate and an OprD family member at the single-molecule level, and they demonstrate the power of single-channel experiments for the quantitative analysis of channel-substrate interactions.

Comparison of OpdK with OprD

OprD and OpdK crystallized as monomers. For OprD, single-channel conductance experiments showed no evidence for oligomerization. However, by using blue-native PAGE in mild detergents, it was shown that OprD does form oligomers, most likely trimers (Biswas et al., 2007). For OpdK, the single-channel experiments suggest that this OM channel forms trimers as well. This notion was confirmed by blue-native PAGE, showing that OpdK incubated in mild detergents has an apparent mobility of ~ 200 kDa, most likely corresponding to a trimer (Figure S1, available online; assuming a micelle molecular weight of ~ 50 kDa). Surprisingly, whereas OprD predominantly forms a trimer in digitonin (Biswas et al., 2007), OpdK is predominantly present as a monomeric species in this detergent. A trimer is in accordance with the presence of two short β strands, S5 and S6 (Figure 1B), which are a structural characteristic of trimeric OM channels

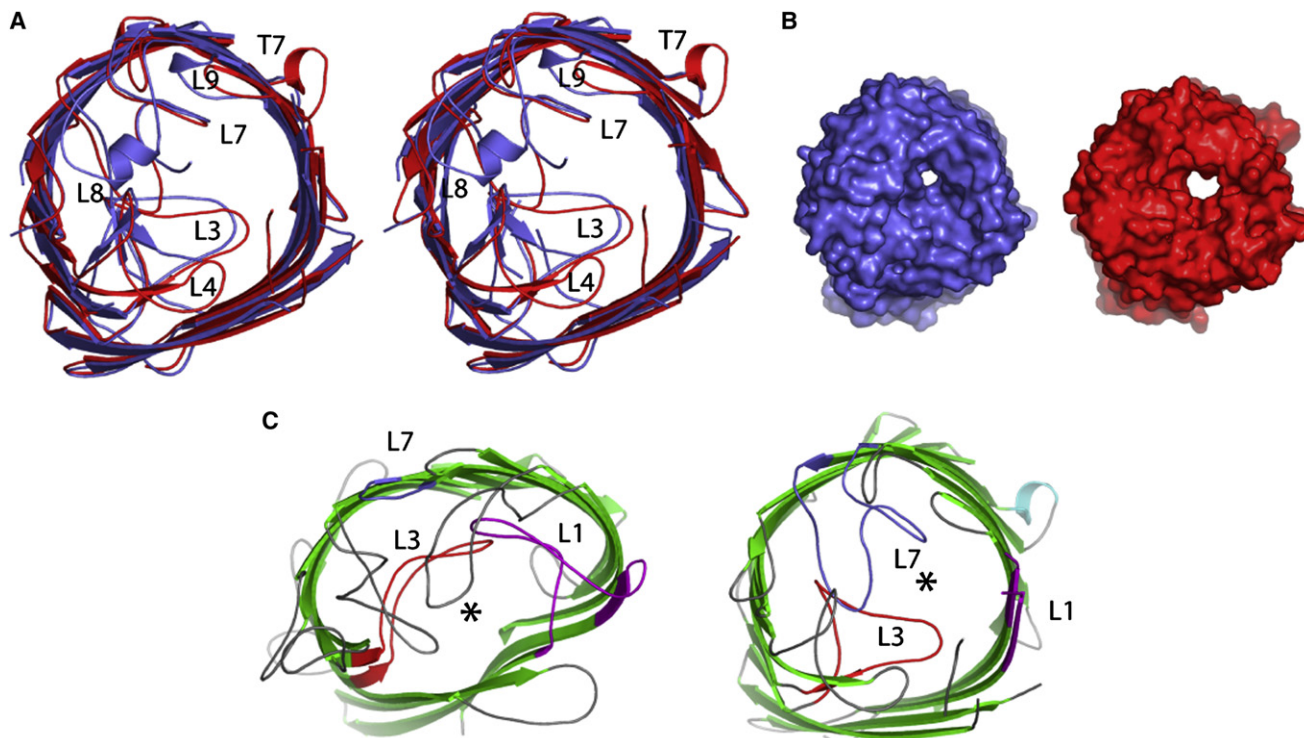


Figure 6. Structural Comparison of OpdK with OprD and LamB

(A) Stereo backbone superposition of OpdK (red) and OprD (blue) made in COOT (Emsley and Cowtan, 2004), showing the similarity in the overall structure. (B) Surface views from the extracellular side, showing the marked difference in shape and dimension between the OpdK (red) and OprD (blue) pores. Orientations are as in (A).

(C) Cartoon view from the extracellular side, showing the dramatic differences between LamB (left panel) and OpdK (right panel). To ease comparison, the two proteins were superposed within COOT. The pore-constricting loops L1 (magenta), L3 (red), and L7 (blue) are shown in different colors for clarity. The pore constrictions are indicated with an asterisk.

(Biswas et al., 2007). We therefore propose that all OprD family members exist as labile trimers within the OM. The reason for the distinctive low stability of OprD channel trimers is not yet clear.

Based on the locations of three groups of conserved amino acids within OprD, we proposed that the OprD structure is representative for that of all OprD family members (Biswas et al., 2007). The crystal structure of OpdK that we report here demonstrates that this notion is likely to be correct. The overall structure of OpdK is very similar to that of OprD (Figure 6A). The largest differences between the two proteins are located in the extracellular loops and the periplasmic turns (loop L8, for example, is much shorter in OpdK). For most of these differences, it is hard to rationalize if they are important for determining the substrate specificity of the two channels. However, one structural difference between OpdK and OprD that is likely to be functionally important is the conformation of the pore-restricting loop L3. The conformation of this loop in OpdK causes its constriction to be substantially wider than in OprD (Figure 6). In addition, a part of loop L7 is shifted in OpdK. Together with the slightly wider barrel diameter of OpdK, these structural differences result in a substantially larger pore for OpdK compared to that of OprD (narrowest diameter of ~ 8 Å, compared to 5.5 Å for OprD). The single-channel conductance of OpdK (~ 350 pS) at physiological pH is 10- to 15-fold higher than that of OprD (~ 28 pS) (Biswas

et al., 2007), which is in agreement with the wider pore present in the OpdK X-ray structure.

What clues does the current apo-crystal structure give about the substrate specificity of OpdK? The residues that line the pore are not dramatically different between OpdK and OprD. In OprD, a basic ladder of arginine and lysine residues likely provides a path for substrate diffusion to and from the pore constriction (Biswas et al., 2007). In OpdK, only three of the six OprD ladder residues are present (R22, R363, and R381; the other three residues are V34, G349, and N365). However, two additional arginine residues line the pore in OpdK (R126 and R158), generating a distinct, positively charged patch on one side of the channel constriction comparable to OprD (Figures 1 and 2). On the opposite side of the pore constriction (relative to the basic residues), OprD has an electronegative pocket that is likely to be important for substrate selection (Biswas et al., 2007). OpdK has a similar charge distribution as OprD, with side chains of D123, S282, D289, and N294 providing an electronegative region on the opposite side of the arginine patch (Figure 2). Thus, the charge distribution of the residues lining the pore is very similar between OpdK and OprD, and it thus does not provide an obvious explanation for the different substrate specificities of these two channels. However, a striking difference between OpdK and OprD exists regarding the surface of the periplasmic funnel leading away from the pore constriction. In OpdK, this surface has a highly

positive charge due to the presence of many lysine and arginine residues that line the funnel (Figure 2C). The electropositive funnel, which is not present on the extracellular side (Figure 2C), is likely to act as a sink for the predominantly negatively charged vanillate molecule, ensuring directional transport into the periplasm from the extracellular environment. Interestingly, the surface of this funnel in OprD has a predominant negative charge instead (Figure 2C), which is in accord with the net positive charge of its substrates, arginine, and other basic amino acids and peptides (Trias and Nikaido, 1990).

Comparison of OpdK with Other Substrate-Specific OM Channels

Although the structures of a substantial number (~35) of β barrel proteins have been solved, there are only a limited number of structures of substrate-specific OM channels: these are the 12-stranded nucleoside transporter Tsx (Ye and van den Berg, 2004), the 14-stranded long-chain fatty acid transporter FadL (van den Berg et al., 2004), the 18-stranded, closely related sugar channels LamB (Schirmer et al., 1995) and ScrY (Forst et al., 1998), and the recently solved structure of the phosphate transporter OprP (Moraes et al., 2007).

To date, the sugar channels are the only other known OM proteins with 18 β strands. Whereas OpdK resembles LamB/ScrY in having the same number of β strands, OpdK is otherwise very different from the sugar channels. First, OpdK appears to form trimers of low stability, whereas the sugar channels form very stable trimers even in SDS at room temperature. Second, the pore architecture and the residues contributing to substrate binding are very different between both types of channels (Figure 6C). Whereas in OpdK the pore constriction is formed by loops L3 and L7 and the barrel wall, in the sugar channels the pore is formed by loop L3 (which has a very different conformation compared to loop L3 of OpdK), loop L1, and the barrel wall (Figure 6C).

LamB and ScrY are characterized by a row of aromatic residues leading to and from the channel constriction (also known as the greasy slide). The aromatic rings of the greasy slide residues interact via van der Waals interactions with the sugar moieties of their substrates (Schirmer et al., 1995). Relative to the greasy slide, the other side of the pore constriction is characterized by rows of positively and negatively charged residues ("ionic tracks") that form hydrogen bonds with the sugar hydroxyl groups. Not surprisingly, very similar contributions of both aromatic and charged residues to substrate binding are observed in the nucleoside transporter Tsx (Ye and van den Berg, 2004). In OpdK, there is no evidence for a greasy slide, which is consistent with biochemical data that OpdK is not specific for sugar-containing substrates. OpdK is instead characterized by an asymmetric charge distribution at the pore constriction, with positively charged residues on one side and an electronegative pocket on the other side (Figure 2).

The phosphate transporter OprP from *P. aeruginosa*, which has 16 β strands and is not related to OpdK, has the smallest pore diameter of any OM channel known to date (~3.5 Å), with a variety of different residues (R133, S125, Y62, R34, and D94) contributing to phosphate binding. OprP has a distinct, seven-step arginine ladder that serves to guide the substrate to the constriction by virtue of its negative charge (Moraes et al., 2007). The

remarkable specificity of OprP for phosphate is achieved by both its long (~9 Å), very narrow channel as well as by the specific chemical nature of the residues at the constriction site. OpdK differs from OprP mainly by having a wider and much shorter constriction, likely making OpdK a less specific channel than OprP.

Conclusions

The current OpdK structure and the recently reported OprD structure firmly establish the general structural architecture of the OprD family and form the starting point for structural, biochemical, and biophysical studies into the mechanism of substrate selectivity and the specificity of a group of closely related OM channels. As the next step, the elucidation of cocrystal structures of OprD channels with their substrates will be required, as well as the development of in vitro transport assays to quantitatively assay substrate specificity of OprD family members. Besides being important fundamentally, such analyses could also be useful for the lead design of novel drugs against *P. aeruginosa* and related Gram-negative bacterial pathogens, by providing information that will allow for and facilitate screening for compounds with better permeability properties.

EXPERIMENTAL PROCEDURES

Cloning, Overexpression, and Purification of OpdK

The OpdK gene was amplified from genomic DNA of *P. aeruginosa* without the signal sequence and was then cloned into pB22 vector (Guzman et al., 1995); the *Serratia marcescens* ShlB signal sequence was present at the N terminus, and an 8-His tag was introduced at the C terminus. The protein was expressed in C43 (DE3) *E. coli* cells. Cells were grown at 37°C for 3 hr until OD₆₀₀ reached ~0.6, and were then induced by 0.2% (w/v) arabinose and grown for 3–4 hr at 30°C. Subsequent steps were performed at 4°C. After harvesting by centrifugation, the cells were resuspended in TSB buffer (20 mM Tris-HCl [pH 8.0], 300 mM NaCl, 10% [v/v] glycerol) and ruptured by two passes at 15,000–20,000 psi (1 psi ≈ 6.9 kPa) in a microfluidizer (Avestin Emulsiflex C-3). Total membranes were obtained by centrifugation at 100,000 × g for 40 min, after which the pellet was resuspended in 1% LDAO in TSB and stirred for 1 hr. This solution was centrifuged at 100,000 × g for 30 min, and the supernatant was loaded onto a Ni-NTA column equilibrated in TSB containing 0.2% LDAO. After washing the column with 15 column volumes of 20 mM imidazole in TSB/0.2% LDAO, the protein was eluted with 250 mM imidazole. The protein was concentrated and loaded on a gel-filtration Superdex-200 26/60 chromatography column (Amersham Biosciences), equilibrated in 10 mM sodium acetate/50 mM NaCl/10% glycerol/0.05% LDAO (pH 5.5). OpdK-containing fractions were pooled, concentrated, and loaded onto a Superdex-200 16/60 chromatography column equilibrated in 10 mM sodium acetate/50 mM NaCl/10% glycerol/0.4% n-octyltetraoxyethylene (C₈E₄) (pH 5.5). OpdK fractions were pooled, concentrated in a Centricon Plus-20 centrifugal filter device (Amicon; 30 kDa Mw cutoff), and dialyzed for ~16 hr at 4°C against 10 mM sodium acetate/50 mM NaCl/10% glycerol/0.4% C₈E₄ (pH 5.5). The protein was concentrated to 7–8 mg/ml (determined by OD₂₈₀, using an E_{1%} of 17), aliquotted, and flash frozen in liquid nitrogen. No measurement was performed to determine any residual amount of LDAO remaining in the protein samples used for crystallization. SeMet-substituted protein was produced in wild-type C43 cells by inhibition of the methionine biosynthesis pathway (van Duyne et al., 1993). Blue-native PAGE was carried out with the Invitrogen NativePAGE Bis-Tris gel system according to manufacturer's instructions, by using a 4%–16% gradient gel. OpdK (4 mg/ml) was purified in 0.4% C₈E₄ as described above, diluted 5- to 20-fold, and incubated for 1 hr at 4°C at concentrations of 0.2–0.8 mg/ml in 10 mM Na-acetate/50 mM NaCl/10% glycerol/0.5% detergent (pH 5.5).

Crystallization, Data Collection, and Refinement

The Se-Met protein crystals grew in 0.2 M ammonium acetate, 0.1 M sodium acetate (pH 6.0), and 30% PEG 4000. The protein concentration used for

Table 1. Data Collection, Phasing, and Structure Refinement Statistics of OpdK

Data Collection and Phasing	
Beamline	NLSL X-29
Wavelength (Å)	0.97960
Resolution range (Å)	50–2.8
Space group	P2 ₁ 2 ₁ 2 ₁
Unit cell dimensions	
a, b, c (Å); α, β, γ (°)	81.9, 96.7, 121.4; 90, 90, 90
Mosaicity (°)	1.0
R _{sym} (%) ^a	15.4 (40.0) ^b
Completeness (%)	98.9 (90.2)
I/σI	18.3 (2.7)
Figure of merit after SOLVE/Z-score	0.28/47
Refinement	
Resolution range (Å)	10–2.8
Total number of atoms (non-hydrogen)	6257
Number of (partial) C ₈ E ₄ molecules	22
R _{work} ^c	23.3
R _{free} ^d	29.5
Rms deviation from ideal	
Bond length (Å)	0.0077
Bond angles (°)	1.37
Average B factor (Å ²)	
Protein main chain/side chain	30.6/32.2
C ₈ E ₄	61.0
Ramachandran plot	
Most favored (%)	79.9
Additionally allowed/disallowed (%)	19.8/0.3

^a $R_{\text{merge}} = \sum(|I - \langle I \rangle|) / \sum(I)$.

^b Values in parentheses are statistics for the highest-resolution shell.

^c $R_{\text{work}} = \sum||F_o| - |F_c|| / \sum|F_o|$ for the 92.5% of reflection data used in refinement.

^d $R_{\text{free}} = \sum||F_o| - |F_c|| / \sum|F_o|$ for the remaining 7.5% of reflection data used in refinement.

crystallization was 7–8 mg/ml. The crystals were grown at 295K by hanging-drop vapor diffusion by mixing 1 μl protein and 1 μl reservoir solution. Rectangular crystals in space group P2₁2₁2₁ appeared within 2 days. Crystals were flash frozen directly from the mother liquor by plunging in liquid nitrogen. The Matthews coefficient (Matthews, 1968) of the crystals is 2.8 Å³/Da, corresponding to a solvent content of 55%. Se-Met-SAD data were collected at 100K on beamline X29 at the National Synchrotron Light Source at Brookhaven National Laboratory. HKL 2000 (Otwinowski and Minor, 1997) was used to scale and index the data. Nine (out of ten) selenium sites were located in the asymmetric unit with SOLVE (Terwilliger, 2004), followed by density modification and two-fold noncrystallographic symmetry (NCS) averaging in RESOLVE (Terwilliger, 2004). The electron density maps were of reasonable quality, and they allowed for automatic building of part of the OpdK model in RESOLVE. The complete OpdK model was built manually in an iterative way by using COOT (Emsley and Cowtan, 2004). Refinement was done in CNS 1.1 (Brunger et al., 1998), and progress was monitored with the R_{free} value, for which a test set comprising 7.5% of the total number of reflections was used. The final model has an R_{free} value of 29.5% and has good stereochemistry, as judged by PROCHECK. The data collection and refinement statistics are summarized in Table 1.

Single-Channel Conductance Experiments

Single-channel recordings on planar lipid bilayers were performed as described previously (Movileanu et al., 2001, 2005). Briefly, 25 μm-thick teflon (Goodfellow Corporation; Malvern, PA) partitioned the two chambers. An aperture of ~80 μm in diameter was pretreated with 10% (v/v) hexadecane (dissolved in high-purity n-pentane). The folding technique was used to form a planar lipid bilayer membrane of 1,2-diphytanoyl-*sn*-glycerophosphocholine (Avanti Polar Lipids; Alabaster, AL) across the aperture. The *cis* and *trans* chambers of the apparatus contained 1.0 M KCl, 10 mM potassium phosphate (pH 7.5). The transmembrane potential was applied through Ag/AgCl electrodes connected to the bath with 1.5% (w/v) agar bridges (Ultra Pure DNA Grade, Bio-Rad Laboratories; Hercules, CA) containing 3 M KCl. The OpdK protein was added to the *cis* chamber, which was at ground. Therefore, a positive single-channel current denotes that the positive charge moves from the *trans* to the *cis* side. Single-channel current was recorded with an Axopatch 200B patch-clamp amplifier (Axon Instruments), in the whole-cell mode (β = 1), with a CV-203BU headstage. All recordings were performed at room temperature. The single-channel signal was low-pass Bessel filtered at 10 kHz with an 8-pole filter (Model 900, Frequency Devices; Haverhill, MA). The single-channel signal was sampled on an Optiplex Dell computer at 100 kHz. Clampex 9.2 (Axon) and ClampFit 9.2 (Axon) were used for data acquisition and analysis, respectively.

As shown previously (Wolfe et al., 2007; Mohammad et al., 2008), single-channel electrical recordings in the presence of a transport substrate enable the simultaneous determination of the rate constants of association (k_{on}) and dissociation (k_{off}) at single-molecule resolution; k_{on} is defined as $1/(c\tau_{\text{on}})$, where τ_{on} is the interevent interval, and c is the concentration of substrate in the *cis* chamber. k_{off} is defined as $1/\tau_{\text{off}}$, where τ_{off} is the mean duration of the transient substrate-induced current blockades. The dissociation constant is given by $K_D = k_{\text{off}}/k_{\text{on}}$.

ACCESSION NUMBERS

The atomic coordinates for OpdK have been deposited in the Protein Data Bank (PDB) with PDB ID code 2QTK.

SUPPLEMENTAL DATA

Supplemental Data include one figure and are available at <http://www.structure.org/cgi/content/full/16/7/1027/DC1>.

ACKNOWLEDGMENTS

The work described in this study was supported by start-up funds from UMass Medical School and a Pew Scholar Research grant (to B.v.d.B.), and by Syracuse University start-up funds and the United States National Science Foundation DMR-0706517 (to L.M.). The authors are also thankful to Khail R. Howard of Syracuse University for his help with single-channel experiments during the early stage of this work. We are indebted to the personnel of National Synchrotron Light Source beamlines X6A and X29 for beamtime and beamline assistance.

Received: January 10, 2008

Revised: March 29, 2008

Accepted: April 1, 2008

Published: July 8, 2008

REFERENCES

- Basle, A., Iyer, R., and Delcour, A.H. (2004). Subconductance states in OmpF gating. *Biochim. Biophys. Acta* 1664, 100–107.
- Bezrukov, S.M., Kullman, L., and Winterhalter, M. (2000). Probing sugar translocation through maltoporin at the single channel level. *FEBS Lett.* 476, 224–228.
- Biswas, S., Mohammad, M.M., Patel, D.R., Movileanu, L., and van den Berg, B. (2007). Structural insight into OprD substrate specificity. *Nat. Struct. Mol. Biol.* 14, 1108–1109.

- Brunger, A.T., Adams, P.D., Clore, G.M., DeLano, W.L., Gros, P., Grosse-Kunstleve, R.W., Jiang, J.S., Kuszewski, J., Nilges, M., Pannu, N.S., et al. (1998). Crystallography & NMR system: a new software suite for macromolecular structure determination. *Acta Crystallogr. D Biol. Crystallogr.* *54*, 905–921.
- DeLano, W.L. (2002). The PyMOL Molecular Graphics System (<http://www.pymol.org>).
- Emsley, P., and Cowtan, K. (2004). Coot: model-building tools for molecular graphics. *Acta Crystallogr. D Biol. Crystallogr.* *60*, 2126–2132.
- Forst, D., Welte, W., Wacker, T., and Diederichs, K. (1998). Structure of the sucrose-specific porin ScrY from *Salmonella typhimurium* and its complex with sucrose. *Nat. Struct. Biol.* *5*, 37–46.
- Guzman, L.M., Belin, D., Carson, M.J., and Beckwith, J. (1995). Tight regulation, modulation, and high-level expression by vectors containing the arabinose PBAD promoter. *J. Bacteriol.* *177*, 4121–4130.
- Hancock, R.E., and Brinkman, F.S. (2002). Function of pseudomonas porins in uptake and efflux. *Annu. Rev. Microbiol.* *56*, 17–38.
- Ishii, J.N., Okajima, Y., and Nakae, T. (1981). Characterization of lamB protein from the outer membrane of *Escherichia coli* that forms diffusion pores selective for maltose-maltodextrins. *FEBS Lett.* *134*, 217–220.
- Maier, C., Bremer, E., Schmid, A., and Benz, R. (1988). Pore-forming activity of the Tsx protein from the outer membrane of *Escherichia coli*. Demonstration of a nucleoside-specific binding site. *J. Biol. Chem.* *263*, 2493–2499.
- Matthews, B.W. (1968). Solvent content of protein crystals. *J. Mol. Biol.* *33*, 491–497.
- Mohammad, M.M., Prakash, S., Matouschek, A., and Movileanu, L. (2008). Controlling a single protein in a nanopore through electrostatic traps. *J. Am. Chem. Soc.* *130*, 4081–4088.
- Moraes, T.F., Bains, M., Hancock, R.E., and Strynadka, N.C. (2007). An arginine ladder in OprP mediates phosphate-specific transfer across the outer membrane. *Nat. Struct. Mol. Biol.* *14*, 85–87.
- Movileanu, L., Cheley, S., Howorka, S., Braha, O., and Bayley, H. (2001). Location of a constriction in the lumen of a transmembrane pore by targeted covalent attachment of polymer molecules. *J. Gen. Physiol.* *117*, 239–251.
- Movileanu, L., Schmittschmitt, J.P., Scholtz, J.M., and Bayley, H. (2005). Interactions of peptides with a protein pore. *Biophys. J.* *89*, 1030–1045.
- Nikaido, H. (2003). Molecular basis of outer membrane permeability. *Microbiol. Mol. Biol. Rev.* *67*, 593–656.
- Otwinowski, Z., and Minor, W. (1997). Processing of X-ray diffraction data collected in oscillation mode. *Methods Enzymol.* *276*, 307–326.
- Schirmer, T., Keller, T.A., Wang, Y.F., and Rosenbusch, J.P. (1995). Structural basis for sugar translocation through maltoporin channels at 3.1 Å resolution. *Science* *267*, 512–514.
- Smith, N., Roitberg, A.E., Rivera, E., Howard, A., Holden, M.J., Mayhew, M., Kaistha, S., and Gallagher, D.T. (2006). Structural analysis of ligand binding and catalysis in chorismate lyase. *Arch. Biochem. Biophys.* *445*, 72–80.
- Tamber, S., Ochs, M.M., and Hancock, R.E. (2006). Role of the novel OprD family of porins in nutrient uptake in *Pseudomonas aeruginosa*. *J. Bacteriol.* *188*, 45–54.
- Terwilliger, T. (2004). SOLVE and RESOLVE: automated structure solution, density modification, and model building. *J. Synchrotron Radiat.* *11*, 49–52.
- Trias, J., and Nikaido, H. (1990). Protein D2 channel of the *Pseudomonas aeruginosa* outer membrane has a binding site for basic amino acids and peptides. *J. Biol. Chem.* *265*, 15680–15684.
- van den Berg, B., Black, P.N., Clemons, W.M., and Rapoport, T.A. (2004). Crystal structure of the long chain fatty acid transporter FadL. *Science* *304*, 1506–1509.
- van Duyn, G.D., Standaert, R.F., Karplus, P.A., Schreiber, S.L., and Clardy, J. (1993). Atomic structures of the human immunophilin FKBP-12 complexes with FK506 and rapamycin. *J. Mol. Biol.* *74*, 105–124.
- Wolfe, A.J., Mohammad, M.M., Cheley, S., Bayley, H., and Movileanu, L. (2007). Catalyzing the translocation of polypeptides through attractive interactions. *J. Am. Chem. Soc.* *129*, 14034–14041.
- Ye, J., and van den Berg, B. (2004). Crystal structure of the nucleoside transporter Tsx. *EMBO J.* *23*, 3187–3195.